IEEE Access
Multidisciplinary | Rapid Review | Open Access Journal

Received April 30, 2020, accepted May 12, 2020, date of publication May 22, 2020, date of current version June 5, 2020.

Digital Object Identifier 10.1109/ACCESS.2020.2996603

A Medical Image Segmentation Method With Anti-Noise and Bias-Field Correction

HONG XU[1,2], CAIZENG YE[1], FAN ZHANG[3], XUEMEI LI[1,4], AND CAIMING ZHANG[1,4]

[1]School of Software, Shandong University, Jinan 250101, China
[2]Shandong Institute of Commerce and Technology, Jinan 250103, China
[3]School of Computer Science and Technology, Shandong Technology and Business University, Yantai 264025, China
[4]Shandong Co-Innovation Center of Future Intelligent Computing, Yantai 264025, China

Corresponding author: Xuemei Li (xmli@sdu.edu.cn)

This work was supported in part by the National Nature Science Foundation of China under Grant 61572292, Grant 61602277, and Grant 61873117, in part by the NSFC Joint Fund with Zhejiang Integration of Informatization and Industrialization through a Key Project under Grant U1609218, and in part by the Natural Science Foundation of Shandong Province under Grant ZR2016FQ12 and Grant ZR2017MF033.

ABSTRACT Brain magnetic resonance images (MRI) are affected by noise and bias field, which make the traditional FCM algorithm unable to segment tissue regions of MR images accurately. Based on the above problems, this paper proposes an MR image segmentation method (MPCFCM) with anti-noise and bias field correction, which implements segmentation by point-to-plane algebraic distance constraint. Different from traditional point-based clustering methods, a hyper-center of clustering (i.e., plane) model is defined, and data clustering is completed by optimizing different planes. In addition, to realize the point clustering with plane, a key problem that how to measure the distance from point to plane needs to be solved. This paper adopts the algebraic distance as a measure function, which can avoid the nonlinear problem caused by a direct calculation of the minimum distance between a point and a plane, thus simplifying the computational complexity. In the proposed algorithm, spatial distance, local variance and gray-difference of neighbors are combined to construct a new anti-noise smoothing factor for constraining the energy function so that the algorithm has better anti-noise and retains more image details. Finally, the singular value decomposition is performed on the loss energy, some information removed is re-added to the segmented image to repair it. The experimental results show that MPCFCM algorithm can better correct bias field and eliminate noise and obtain accurate image segmentation results with more details.

INDEX TERMS Bias field correction, fitting plane, algebraic distance, anti-noise smoothing factor.

I. INTRODUCTION

Image segmentation is very important in computer vision and medical image processing. It aims to segment the image into disjoint and different regions, and makes the pixels in the same region be with the same or similar features. At present, medical magnetic resonance imaging (MRI) segmentation mainly focuses on the segmentation of gray matter (GM), white matter (WM) and cerebro-spinal fluid (CSF) in brain tissue. However, due to the interference of various external factors such as uneven illumination, noise and so on, medical images have a certain degree of fuzziness, which increases the difficulty of accurate segmentation. In order to segment the object rapidly and accurately, various image segmentation algorithms have been developed in the literature. Such as [1], [2], [4]–[13] based on clustering algorithm, [14]–[16] based on level set method, and [21]–[26] based on deep learning method.

Among the clustering-based image segmentation methods, the most classical one is the Fuzzy C-means (FCM) algorithm, which was proposed by Bezdek in 1973 [1]. The core of this method is a fuzzy clustering algorithm based on an objective function, which is composed of membership (an indicator for evaluating the similarity degree of a sample and different clustering results) and the Euclidean distance from a sample point to each class center. The basic idea is to specify the number of clustering centers, in which the distance from a sample point to the clustering center is inversely proportional to its corresponding membership. When the objective function reaches its minimum, it means the algorithm stabilizes gradually in the iteration minimization process of the objective function and the segmentation result is satisfactory.

The associate editor coordinating the review of this manuscript and approving it for publication was Md. Asikuzzaman.

Although FCM algorithm can retain as much information as possible, it is greatly affected by noise and intensity inhomogeneity.

In order to strengthen the relationship between spatial neighborhood information, Ahmed *et al.* [2] modified the objective function of FCM algorithm and proposed an algorithm named FCM_S algorithm. This algorithm can suppress noise to a certain extent, but it is inefficient and time-consuming because of the computation neighborhood information in each iteration process [3]. Chen and Zhang [4] proposed two variant algorithms (FCM_S1 and FCM_S2) to reduce the time complexity of the algorithm by using mean-filter and median-filter respectively to deal with the influence between pixels in each neighborhood window. Szilagyi *et al.* [5] proposed a fast FCM clustering algorithm based on image gray level, named EnFCM algorithm, which reduces the time complexity by calculating the linear weighting of the original image and the average gray level of the local neighborhood. Krinidis and Chatzis [6] proposed an algorithm named FLICM algorithm to solve the shortcoming of manually setting parameters in image processing. This algorithm can control the weight between smoothing and preserving the details by adjusting the parameters adaptively, combining with the local information, and introducing a fuzzy factor, which can effectively suppress the influence of noise.

In medical image processing, the more popular algorithms include breast cancer detection algorithms [7]–[12], [17], level set segmentation algorithms [14]–[16], bias correction methods based on Fuzzy C-means [18]–[20] and so on. In particular, Chowdhary and Acharjya *et al.* [17] proposed a novel intuitionistic possible Fuzzy C-means algorithm, which mixed the possible Fuzzy C-means with the intuitionistic Fuzzy C-means to overcome the coincidence cluster problem, and reduced the sensitivity of outliers while reducing the noise. Although these algorithms can process medical images effectively, due to the shortcomings of the algorithm itself, it is necessary to further improve the algorithm to obtain better segmentation results. In addition, deep convolution neural network is also popular in image segmentation. It has been successfully applied in natural image [21] and medical image [22], [23], especially in brain tumor image segmentation [24]–[26]. Compared with traditional methods, these methods based on deep learning have their unique advantages and can well deal with the impact of noise on image segmentation. However, its model structure is complex, and it needs to find suitable hyper parameters and the training time is also relatively high.

In order to segment the image more accurately, we redefine the objective function of the traditional algorithm, fully consider the influence of bias field and combine the local information and the neighborhood information to design a new anti-noise smoothing factor to enhance the image denoising effect, and after the initial segmentation image post-processing to ensure the integrity of their segmentation image information. Therefore, based on the above strategy, this paper designs a medical image segmentation model with anti-noise and bias field correction. The main contributions of this paper are summarized as follows:

1) A new algorithm based on FCM algorithm for bias field correction and segmentation of brain MR images is proposed. We defined a new objective function, added a bias field estimation model and first proposed a polynomial fitting plane as a clustering center to improve the accuracy of image segmentation;

2) A new anti-noise smoothing factor model is proposed. It is constructed by combining the variance coefficient of the local window and the neighborhood window gray-scale difference coefficient to suppress the influence of noise;

3) The singular value decomposition is adopted to supplement the part of image information lost in the process of removing bias field, and the lost energy function is added into the initial segmentation result of the image to obtain the final segmentation result.

The experimental results show that the new image segmentation method improves the robustness of bias field correction and the accuracy of tissue segmentation. The remainder of this paper mainly focuses on the following four parts. Section II is the introduction of related algorithms. Section III is the detailed introduction of the new algorithm proposed in this paper. Section IV is the demonstration of our experimental results and the conclusion of Section V.

II. RELATED WORKS

A. RELATED FCM ALGORITHM

The traditional FCM algorithm achieves segmentation by updating the membership and clustering centers and minimizing the objective function iteratively to be stable. The objective function of FCM algorithm is defined as follows:

$$E_{FCM} = \sum_{k=1}^{C} \sum_{i=1}^{N} u_{ki}^{m} ||x_i - v_k||^2, \tag{1}$$

where C is the clustering number, N is the total number of image pixels, m is the fuzzy weight coefficient. The clustering validity problem shows that value range of m is [1.5,2.5]. Based on many experiments and analyses, m=2 is the simplest and the most effective approach. u_{ki} represents the fuzzy membership of the i-th pixel x_i relative to the k-th clustering center v_k. $||x_i - v_k||$ is the Euclidean distance between x_i and v_k. The value range of membership is [0,1], and the sum of fuzzy membership of pixels belonging to different clusters is 1. Namely,

$$\sum_{k=1}^{C} u_{ki} = 1, \quad u_{ki} \in [0, 1], \tag{2}$$

In formula (1), FCM algorithm calculates the membership of each pixel in the image by minimizing the objective function. However, this objective function does not take the spatial neighborhood information of pixels into consideration, which results in the image being sensitive to noise information and therefore can not get perfect segmentation effect. To solve

this problem, FCM_S algorithm adds spatial neighborhood information into FCM algorithm, and its objective function is defined as follows:

$$E_{FCM\_S} = \sum_{k=1}^{C}\sum_{i=1}^{N} u_{ki}^{m}||x_i - v_k||^2 + \frac{\alpha}{N_R}\sum_{k=1}^{C}\sum_{i=1}^{N} u_{ki}^{m}\Big(\sum_{x_j\in N_i}||x_j - v_k||\Big)^2, \quad (3)$$

where α is the parameter used to control the neighborhood term. Larger α value indicates bigger impact of local space constraint term in the clustering process. Conversely, the role of local space constraints is smaller. N_R represents the number of neighborhood points, and N_i represents the neighborhood point in the i-th neighborhood window. Although the algorithm achieves satisfactory results when dealing with noisy MR images, it is computationally inefficient because of the requirement of a great deal of neighborhood information calculation for each iteration. In order to solve the above problem, FLICM algorithm introduces a fuzzy anti-noise factor and controls the trade-off between smoothing and clustering by adaptively adjusting parameters, which is defined as follows:

$$G_{ki} = \sum_{j\in N_i}\frac{1}{d_{ij}+1}\left(1-u_{kj}\right)^m||x_j - v_k||^2, \quad (4)$$

where pixel x_i is the center pixel of the local window, and the pixel x_j is a collection of neighboring pixels centered on the pixel x_i. d_{ij} is the Euclidean distance between the central pixel x_i and the pixel x_j. Combined with the new impact factor G_{ki}, the objective function in FLICM algorithm is defined as:

$$E_{FLICM} = \sum_{i=1}^{N}\sum_{k=1}^{C}\left(u_{ki}^{m}||x_i - v_k||^2 + G_{ki}\right). \quad (5)$$

FLICM algorithm controls the weighting between noise removal and retention details by adaptively adjusting parameters. It does not need to be manually adjust the parameters, the adaptability is enhanced. Also because of the impact factor G_{ki}, noise pixels falling into the window have a similar value to cluster center pixel, the algorithm has better performance of refraining noise. However, with regard to the non-uniform illumination, it is difficult to segment the image successfully.

B. BIAS FIELD AND ITS MODELING

1) OVERVIEW OF BIAS FIELD

Magnetic resonance imaging (MRI) is a non-destructive way for three-dimensional tomography human detection, which is often used to detect abnormalities in soft tissue. However, due to the imperfect MRI equipment and the specificity of the object itself, MR images inevitably have a certain degree and range of brightness unevenness [27], which is called bias field. Bias field is a smooth, slowly varying multiplicative field that changes the local statistical properties of the image. Among them, the brightness information of the image is the main basis of image post-processing, but the overlapping of the brightness of different physiological tissues is the obstacle of image post-processing. This situation seriously influences the accuracy of automatically processing MR images. Therefore, correcting bias field is an indispensable step in the post-processing of MR images. MR images of brain are mainly affected by smoothly varying bias field, and thereby the gray values of the same tissue is varied with different position.

2) BIAS FIELD MODELING

In medical images, bias field is embodied by the fact that the pixel gray of the same tissue on the image exhibits a slow and smooth change in space, which can be regarded as a multiplication term in the medical image. Therefore, the observed image can be expressed as [28] :

$$I(x) = b(x)I_0(x) + N(x), \quad (6)$$

where $I(x)$ is the intensity of pixel x in the original image, $I_0(x)$ is the real image to be restored, $b(x)$ is bias field in the original image, and $N(x)$ is zero mean additive noise. The process of bias field correction is to detect and remove bias field $b(x)$ from the original image $I(x)$. According to formula (6), the original image I can be decomposed into two multiplicative terms b, I_0, and one additive noise N. We can consider the estimation of bias field and tissue segmentation as an energy minimization problem, that is, to seek an optimal segmentation of the original image I with respect to bias field b and the real image I_0. Bias field can be defined as a linear combination of a set of given basis functions [29] $g_1(x)\ldots g_M(x)$ to guarantee the smooth variation of bias field. when using a large enough number of basis functions M, a function can be approximately expressed as a linear combination of basis functions with arbitrary accuracy. In MR images of 1.5T and 3T, 15 polynomials can be used as the basis function. Based on the above theoretical research, the linear combination of bias fields can be defined as follows:

$$b(x) = \sum_{k=1}^{M} w_k g_k(x). \quad (7)$$

The purpose is to find a set of optimal coefficients $w_1\ldots w_M$ in the set of linear combinations, and represent the set of coefficients as a column vector $w = (w_1\ldots w_M)^T$, and the basis functions $g_1(x)\ldots g_M(x)$ are represented as a column vector function $G(x) = (g_1(x)\ldots g_M(x))^T$, so bias field $b(x)$ is represented as the following vector form:

$$b(x) = w^T G(x). \quad (8)$$

$I_0(x)$ is obtained by multiplying the given membership $u_i(x)$ and the cluster center c_i, so the real image $I_0(x)$ is defined as follows:

$$I_0(x) = \sum_{i=1}^{N} c_i u_i(x). \quad (9)$$

Based on the inherent properties of bias field and the real image, the objective function can be obtained as follows:

$$F(b, I_0) = F(u, c, w) = \int_{\Omega} |I(x) - w^T G(x) \sum_{i=1}^{N} c_i u_i(x)|^2 dx. \quad (10)$$

where $G(x)$ is the basis function, $u = (u_1, \ldots, u_N)^T$, $c = (c_1, \ldots, c_N)^T$ and $w = (w_1, \ldots, w_N)^T$ are three variables that need to be determined.

III. DETAILED ALGORITHMS

In FCM segmentation algorithm and its improved algorithms, the basic idea is to use points as the cluster center, and the basic form of the algorithm is shown in formula (1). By minimizing the objective function, the cluster center and membership are calculated. The result of point clustering is a set of data points with the same mark as the clustering center. But sometimes the segmentation result will be deviated, and the satisfactory result cannot be obtained. This paper defines a hyper-center of clustering (i.e., plane), completes data clustering by optimizing different planes and finishes the automatic segmentation with the constraint of the point-to-plane algebraic distance. In addition, in order to reduce the influence of noise, a new anti-noise smoothing factor is constructed to suppress the influence of noise. Finally, singular value decomposition [30] is adopted to supplement the lost image energy and retain more image details.

A. HYPER-CENTER OF CLUSTERING

The key problem of traditional clustering segmentation algorithms are how to determine the clustering center and impose constraints on the energy function. Typical segmentation methods based on point clustering take ''data points'' as the clustering center. By calculating the distance from each point to the ''center point'' to determine which class the pixel belongs to. Its essence is the data classification. The results of clustering are data sets that have the same marks with their clustering centers. But these constant-centric clustering algorithms sometimes fail to achieve ideal or even getting misleading results. For example, when data points are sampled from different planes, as shown in FIGURE 1, the test data in (b) is sampled from three intersecting planes (a).

It can be seen from the above experiments that when the data points are sampled from different planes, defining the cluster center as a plane can obtain a good clustering effect, as shown in (c). The method of using points as the cluster center produces obvious erroneous results, as shown in (d). In the process of medical image segmentation, hyper-center of clustering algorithm also shows the advantage of high segmentation accuracy.

Based on the above analysis, hyper-center of clustering algorithm realizes data point clustering by optimizing different plane coefficients. The essence is to construct different planes to fit the scattered data points. The results of clustering

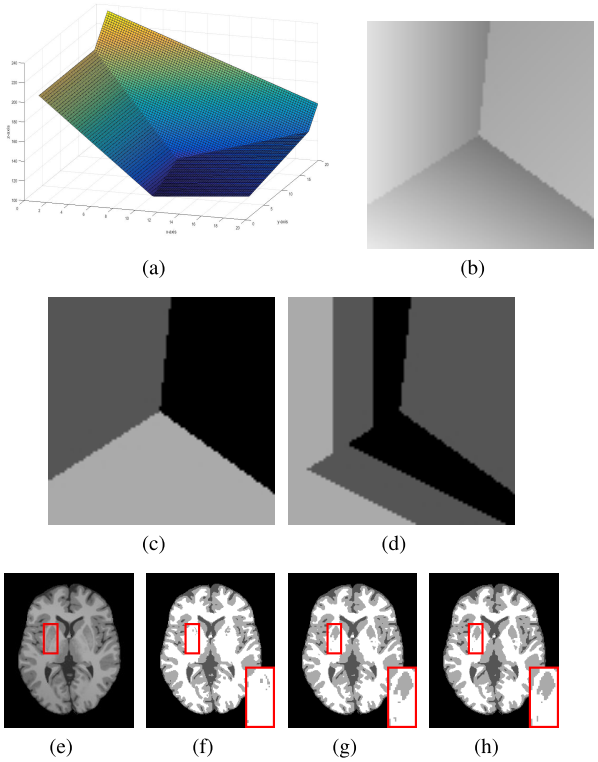

FIGURE 1. Algorithm analysis results. (a) A curved surface obtained by combining three planes; (b) The images sampled on the combined surface; (c) Plane clustering segmentation result; (d) Point clustering segmentation result; (e) Brain MR Image; (f) Point clustering segmentation result; (g) Plane clustering segmentation result; (h) Ground truth.

are planes with different coefficients. In this paper, hyper-center of clustering is defined as follows:

$$f_k(x_i, y_i) = a_{k0} x_i + b_{k1} y_i + c_{k2}. \quad (11)$$

where a_{k0}, b_{k1}, c_{k2} are the coefficients of the k-th plane in the fitting plane f, x_i and y_i are the horizontal and vertical coordinate positions of the current pixel respectively. The points are clustered to a plane. The key problem to be solved is how to measure the distance between point to plane. Calculating the minimum distance directly is more likely to have nonlinear problems, which increases the complexity of the algorithm. In this paper, the point-to-plane algebraic distance is used as a measure function to simplify the complexity of the problem.

B. NEW SMOOTHING FACTOR OF NEIGHBORHOOD WINDOW

In order to make the classification more accurate, this paper introduces a new smoothing factor. By better measuring the local similarity to increase the constraint on the energy function, the algorithm has better anti-noise while retaining more image details. In the relative area of the image, the value of smoothing factor is relatively small and the large by contraries. In the clustering process, in order to effectively characterize the influence of neighboring pixels on the central

pixel, a new smoothing factor is defined by spatial distance, local variance and neighborhood gray difference. Due to the use of local variance and neighborhood gray difference, the anti-noise performance of the new smoothing factor is enhanced.

In [6], the spatial distance factor from the neighborhood pixel to the center pixel is defined as follows:

$$\ell_{sd} = \frac{1}{d_{ij} + 1}. \tag{12}$$

Where d_{ij} is the Euclidean distance between the center pixel i of the local window (3×3) and the neighbor pixel j. Obviously, formula (12) is not a good measure of smoothness. Because of the existence of noise, the neighborhood pixels are often corrupted by different degrees of noise. In order to reduce the influence of noise on the clustering results, the corresponding smoothness of neighborhood pixels with high noise corrupted should be small. In addition, if the neighborhood pixel is at the edge of the object, a small smoothness value should also be given. The local variance of the neighborhood pixel and the gray-difference of the neighborhood pixel can measure the edge property of the pixel and the degree of noise corrupted.

The size of the local variance determines the contrast of the local area. For noisy images, areas with large contrast are often affected by noise. The local variance factor is defined as follows:

$$P_u = \frac{\Re(x)}{(\bar{x})^2}. \tag{13}$$

where $\Re(x)$ is the gray-scale variance in the neighborhood window centered on pixel j, and $\bar{x}$ represents the average of the gray levels in the local window.

Secondly, the neighborhood gray-difference coefficient reflects the similarity of gray value between neighborhood pixel and center point. The neighborhood gray-difference coefficient is defined as follows:

$$S_{ij} = \left\| x_j - x_i \right\|^2, \quad j \in N_i \tag{14}$$

where j is the neighborhood pixel, i is the central pixel, and S_{ij} represents the gray-difference between the j-th pixel and the central pixel i.

Finally, we unify the data dimension and normalize the local variance coefficient $\mathcal{K}_i$ and the neighborhood gray-difference coefficient φ_{ij} to (0, 1], the purpose of which is to balance the effect of two quantities on energy effectively. Normalized $\mathcal{K}_i$ and φ_{ij} are defined as follows:

$$\kappa_i = \frac{(P_u - P_{\min}) + \zeta}{(P_{\max} - P_{\min}) + \zeta} \tag{15}$$

$$\varphi_{ij} = \frac{\left(S_{ij} - S_{ij(\min)}\right) + \zeta}{\left(S_{ij(\max)} - S_{ij(\min)}\right) + \zeta} \tag{16}$$

where $P_{\min}$ represents the minimum value of the local variance in the neighborhood window, and $P_{\max}$ represents the maximum value. Similarly, $S_{ij(\min)}$ represents the minimum value of the local gray-difference coefficient in the neighborhood window, and $S_{ij(\max)}$ represents the maximum value. The value range of the parameter ζ is (0,1]. In this article, in order to ensure that the values of $\mathcal{K}_i$ and φ_{ij} are not zero, so $\zeta = 0.001$.

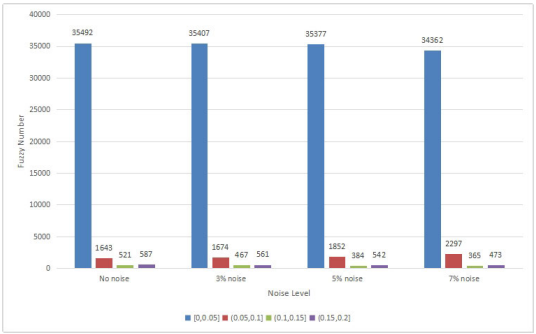

(a)

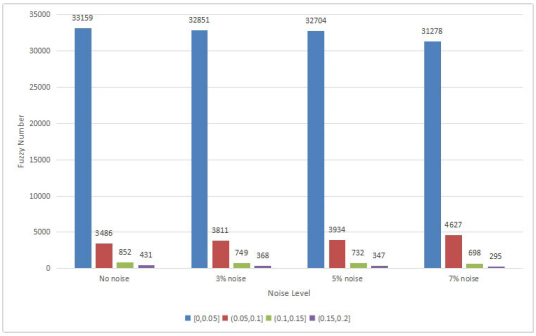

(b)

FIGURE 2. Comparison of two anti-noise factors. (a) The distribution of smoothing factor $\hbar_{sc}$ in MPCFCM algorithm. (b) The distribution of fuzzy factor δ_{sc} in RCLFCM algorithm.

Therefore, the new smoothing factor is defined as follows:

$$\hbar_{sc} = (1 - log_2(1 + \sqrt{\kappa_i})) \times (1 - log_2(1 + \sqrt{\varphi_{ij}})), \quad j \in N_i \tag{17}$$

To illustrate the effectiveness of the new smoothing factor $\hbar_{sc}$, we compared $\hbar_{sc}$ with the fuzzy factor δ_{sc} in [33]. Use formula (17) to calculate the smoothing factors of no noise, 3% noise, 5% noise, and 7% noise images, and count the number of smoothing factor in the interval [0,1]. Since the number of smoothing factor in the interval (0.2,1] is relatively small, we do not analyze it and only compare the smoothing results in the interval [0,0.2]. When noise is added to images, a good smoothing operator can maintain the distribution of smoothing factor in the original image to the greatest extent. FIGURE 2 shows the distribution of smoothing factor in MPCFCM and RCLFCM algorithms after adding noise (3%, 5%, 7%). It can be seen from the histogram that with the increase of noise, the difference between the smoothing factor distribution of MPCFCM and the smoothing factor distribution in the original image is relatively small, especially the number of flat regions has not decreased significantly.

However, the distribution of the fuzzy factor of RCLFCM in different noise conditions is quite different from the distribution of the smoothing factor in the original image, and with the increase of noise, the smoothness retention ability decreases rapidly, and the anti-noise effect is not ideal. Therefore, the smoothing factor in MPCFCM can better suppress noise. In addition, the experiments in Section IV also show the better anti-noise of our algorithm.

In summary, by combining with the spatial distance factor, algebraic distance factor and new smoothing factor, the impact factor of the objective function is defined as follows:

$$\begin{aligned}\vartheta_{ij} &= \ell_{sd} \times \hbar_{sc} \\ &= \frac{1}{d_{ij}+1} \times (1 - log_2(1+\sqrt{\kappa_i})) \\ &\quad \times (1 - log_2(1+\sqrt{\varphi_{ij}})).\end{aligned} \tag{18}$$

The newly proposed impact factor not only considers the spatial distance and algebraic distance, but also considers the neighborhood window variance coefficient and gray scale coefficient, which more comprehensively measures the degree of influence of the neighborhood information points on the central pixel. Compared with other algorithms, the new method proposed in this paper can better suppress the influence of noise and maintain more accurate image details.

C. ENERGY MINIMIZATION EQUATION COMBINED WITH BIAS FIELD

After the newly defined anti-noise smoothing factor is added, the objective function of the biased field with a plane as the clustering center is defined as follows:

$$J_{MPCFCM} = \sum_{i=1}^{N}\sum_{k=1}^{C}\left(u_{ki}^{m}\left\|b_i f_k - P_i\right\|^2 + G_{ki}\right), \tag{19}$$

$$G_{ki} = \sum_{j\in N_i}\vartheta_{ij}\left(1-u_{kj}\right)^m\left\|b_i f_k - P_j\right\|^2, \tag{20}$$

where b_i is bias field intensity of the current pixel P_i, f_k is the currently defined fit plane, u_{ki} represents the fuzzy membership of the i-th pixel relative to the k-th plane function. P_i is the gray value of the current pixel i, P_j is a pixel that falls into a neighborhood window centered on the P_i. ϑ_{ij} is the newly defined impact factor.

By fixing the values of two variables, the algorithm minimizes the objective function to calculate another variable and iteratively solves three variables in turn. The entire iterative process is performed under the constraint $0 \le u_{ki} \le 1$ and $\sum_{k=1}^{C} u_{ki} = 1$. Therefore, u_{ki} and the fitting plane coefficients a_{k0}, b_{k1} and c_{k2} are obtained by minimizing the objective function, and the specific calculation formula is as follows:

$$u_{ki} = \frac{1}{\sum_{l=1}^{C}\left(\frac{\|f_k-P_i\|^2+G_{ki}}{\|f_l-P_i\|^2+G_{li}}\right)^{\frac{1}{m-1}}}, \tag{21}$$

$$\begin{cases}\dfrac{\partial F}{\partial a_{k0}} = \displaystyle\sum_{i=1}^{N} u_{ki}^{m} b_i x_i\left(b_i f_k - P_i\right) \\ \quad + \displaystyle\sum_{j\in N_i}\vartheta_{ij}\left(1-u_{kj}\right)^m b_i x_i\left(b_i f_k - P_j\right) = 0 \\ \dfrac{\partial F}{\partial b_{k1}} = \displaystyle\sum_{i=1}^{N} u_{ki}^{m} b_i y_i\left(b_i f_k - P_i\right) \\ \quad + \displaystyle\sum_{j\in N_i}\vartheta_{ij}\left(1-u_{kj}\right)^m b_i y_i\left(b_i f_k - P_j\right) = 0 \\ \dfrac{\partial F}{\partial c_{k2}} = \displaystyle\sum_{i=1}^{N} u_{ki}^{m} b_i\left(b_i f_k - P_i\right) \\ \quad + \displaystyle\sum_{j\in N_i}\vartheta_{ij}\left(1-u_{kj}\right)^m b_i\left(b_i f_k - P_j\right) = 0\end{cases} \tag{22}$$

$$\begin{bmatrix} a_{k0} \\ b_{k1} \\ c_{k2}\end{bmatrix} = X\begin{bmatrix} x_i \\ y_i \\ 1\end{bmatrix} \tag{23}$$

where,

$$X = \frac{\sum_{i=1}^{N} b_i\left(u_{ki}^{m}P_i + \sum_{j\in N_i}\vartheta_{ij}\left(1-u_{kj}\right)^m P_j\right)}{\sum_{i=1}^{N} b_i^2\left(u_{ki}^{m} + \sum_{j\in N_i}\vartheta_{ij}\left(1-u_{kj}\right)^m\right)} \tag{24}$$

We define the intensity of bias field as a linear combination $b_i = w^T G(i)$, where the coefficients are the column vectors $w = (w_1, \ldots, w_M)^T$, $G(i)$ is the basis function represented by the column vector function $G(i) = (g_1(i), \ldots, g_M(i))^T$, we fix the variable u_{ki} and the plane coefficients, and then calculate bias field by deriving w from objective function F and minimize its energy. The partial derivative of F with respect to w is equal to 0, and we get:

$$\frac{\partial F}{\partial w} = -2V + 2Aw = 0, \tag{25}$$

where,

$$\begin{cases} V = \int_{\Omega} G(i)I(i)\left(\displaystyle\sum_{i=1}^{N}\sum_{k=1}^{C} f_k u_{ki}^{m}(i)\right)di, \\ A = \int_{\Omega} G(i)G(i)^T\left(\displaystyle\sum_{i=1}^{N}\sum_{k=1}^{C} f_k^2 u_{ki}^{m}(i)\right)di.\end{cases} \tag{26}$$

The updated formula for the coefficient w is as follows:

$$w = \frac{\sum_{i=1}^{N}\sum_{k=1}^{C} G(i)u_{ki}^{m} f_k P_i}{\sum_{i=1}^{N}\sum_{k=1}^{C} G(i)G(i)^T u_{ki}^{m} f_k^2}. \tag{27}$$

Finally, we estimate the value of bias field through the definition of the above equation w, and the formula is as follows:

$$b_i = w^T G(i). \tag{28}$$

D. POST-PROCESSING OF IMAGE SEGMENTATION

The bias field estimation model is added to the objective function to correct the bias field while MR image segmentation, which can suppress the influence of uneven intensity on segmentation results effectively. However, while removing the bias field, it is inevitable to lose some useful information

in the image. The algorithm uses the singular value decomposition method to obtain the missing information and add it back to the image. The specific process is as follows:

If $I(x)$ is the intensity of original image, $I_0(x)$ is the real image to be restored, the energy lost due to bias correction can be approximately expressed as:

$$B(x) = I(x) - I_0(x). \tag{29}$$

In addition to bias field, this part of the lost energy usually contains part of the image information. In this paper, low-rank approximation based SVD [30] is adopted to deal with this part of the lost energy. The loss energy function of image information caused by removing bias field is defined as follows:

$$E(x) = B(x) - LRA(B(x)). \tag{30}$$

The image information loss energy function E is added to the segmentation result to get the final segmentation image:

$$J'(x) = \sum_{k=1}^{C} f_k u_k(x) + E(x). \tag{31}$$

Algorithm 1 *MPCFCM* $(a_{k0}, b_{k1}, c_{k2}, m, p, \tau)$

Input: Image J with n pixels, the number C of the clusters, termination threshold τ, fuzzy weighted index m and parameter p.

1: Initialize the membership matrix M and the fitting plane coefficients a_{k0}, b_{k1}, c_{k2} ;
2: Set the loop counter n=0;
3: Update b_i in (28);
4: Update a_{k0}, b_{k1}, c_{k2} in (23);
5: Update u_{ki} in (21);
6: **if** $\left(M^{(n)} - M^{(n+1)}\right) \geq \tau$ **then**
7: n=n+1; go to step 3;
8: **else**
9: Update B in (29);
10: Update E in (30);
11: Update J' in (31);
12: stop;
13: **end if**

Output: the membership value u_{ki}, the fitting plane coefficient a_{k0}, b_{k1}, c_{k2}, the estimation of bias field b_i when the algorithm converges and Image J' after segmentation.

Algorithm implementation steps are shown in Algorithm 1. The algorithm of this paper can be interpreted as an iterative process. Three variables of the algorithm: bias field, clustering plane coefficient and fuzzy membership are updated alternately in the iteration. Each variable is calculated on the basis of the other two variables. the algorithm termination condition is based on the fact that the membership value change of two consecutive iterations is less than the termination condition τ ($\tau = 0.0001$). When the algorithm converges, the membership matrix is defuzzed according to the principle of maximum membership division. Divide each pixel into its own clustering plane and add loss energy function, finally bias field corrected and segmented image is obtained.

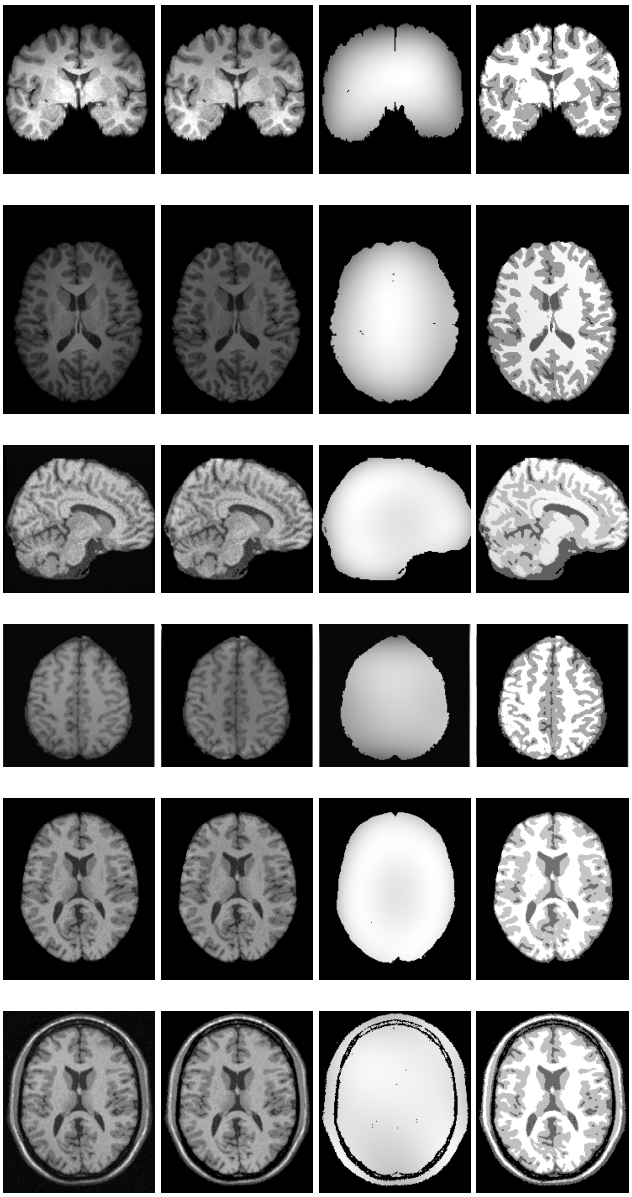

FIGURE 3. Experimental results of MPCFCM algorithm. (a) Three actual 3T brain MR images; (b) bias field corrected images; (c) estimated bias field; (d) experimental segmentation results.

IV. EXPERIMENTAL RESULTS

This section evaluates the effectiveness of our medical image segmentation method. The test images for the experiments are all from the Brain Web database [31]. The image database contains all the data of brain simulation and anatomical model, which can provide a variety of different slice thickness, noise level and bias field level. We divide this section into two parts. First, we give our experimental results in the first part, and test the performance of the proposed scheme on

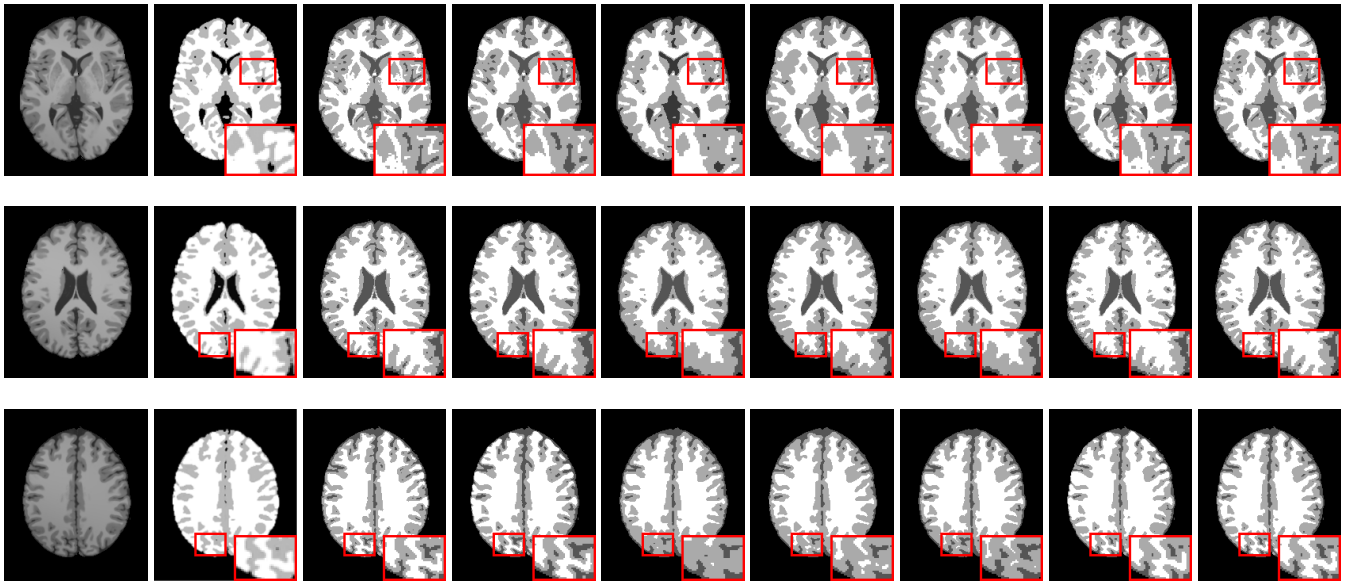

FIGURE 4. Comparison of segmentation results for different algorithms. (a) T1-weighted, 1mm thickness and 40% bias field brain MR original image; (b) LINC; (c) MICO; (d) RCLFCM; (e) NLFCM; (f) FRFCM; (g) DSFCM_N; (h) MPCFCM; (i) Ground truth.

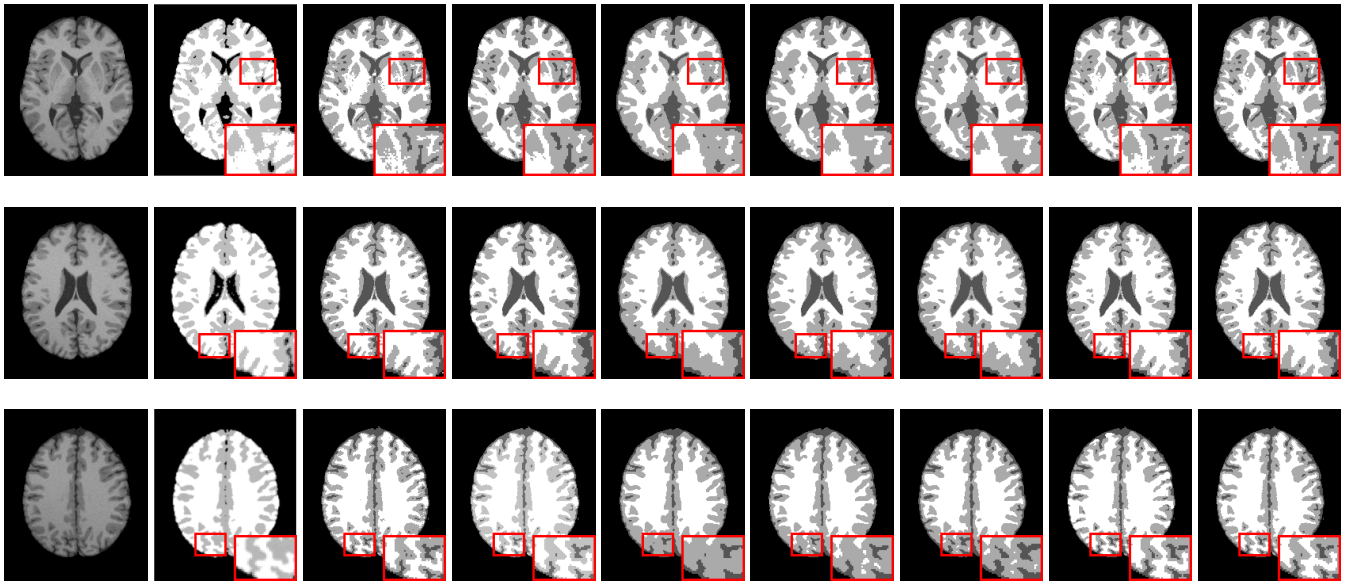

FIGURE 5. Comparison of segmentation results for different algorithms. (a) T1-weighted, 1mm thickness, 40% bias field and 3% Gaussian noise image of the brain MR image; (b) LINC; (c) MICO; (d) RCLFCM; (e) NLFCM; (f) FRFCM; (g) DSFCM_N; (h) MPCFCM; (i) Ground truth.

twenty brain images. Among them, the six images show the correction of bias field and the segmentation result respectively, and the other fourteen images compare the segmentation result with six segmentation algorithms. The next part is quantitative evaluation.

A. VISUAL EFFECT OF SEGMENTATION

In order to demonstrate that the new method (MPCFCM) in this paper has a good ability to deal with uneven intensity, we apply MPCFCM to six images shown in the left column of FIGURE 3. The corrected images of bias field, estimated bias field and segmentation results are shown in the second, third and fourth columns respectively. Despite the uneven intensity of the image, our method can produce better results of bias field correction and tissue segmentation, and the experimental results are shown in FIGURE 3.

Compare MPCFCM with several other popular algorithms, including: LINC [15], MICO [32], RCLFCM [33], NLFCM [34], FRFCM [35] and DSFCM_N [36].

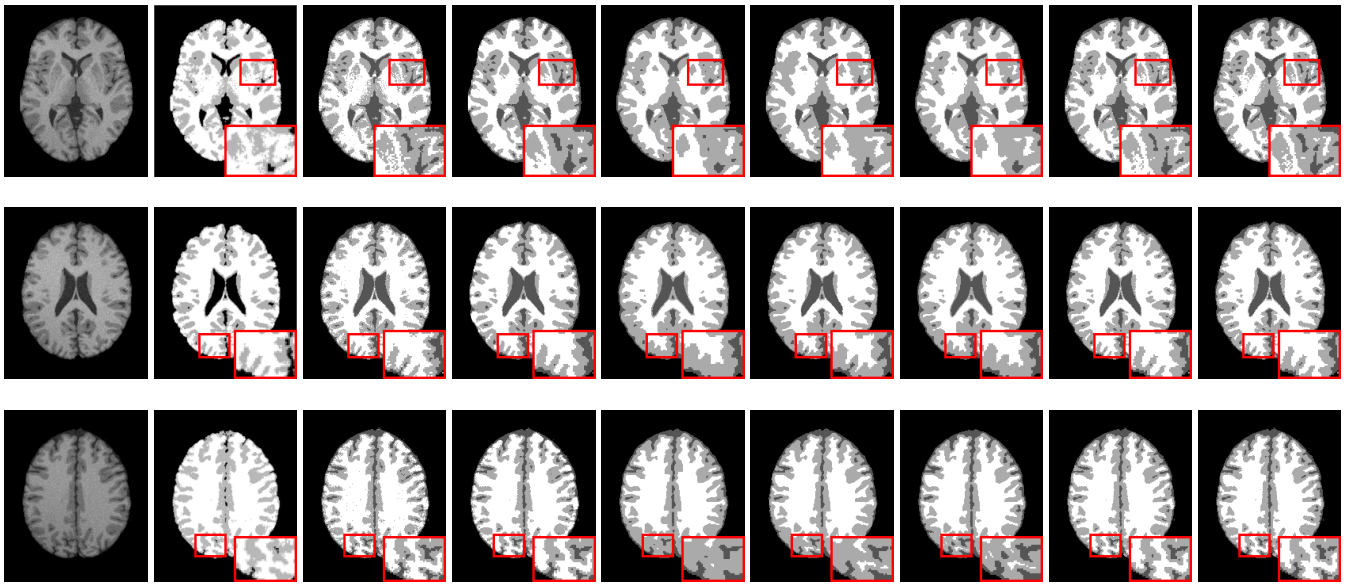

FIGURE 6. Comparison of segmentation results for different algorithms. (a) Brain image of T1-weighted, 1mm thickness, 40% bias field and 5% Gaussian noise; (b) LINC; (c) MICO; (d) RCLFCM; (e) NLFCM; (f) FRFCM; (g) DSFCM_N; (h) MPCFCM; (i) Ground truth.

FIGURE 4 shows the segmentation results of brain synthetic image where the image has a bias field value of 40%, a T1 sequence, and a thickness of 1 mm. It can be seen from the experimental results that LINC, NLFCM, FRFCM and DSFCM_N are not accurate enough due to the influence of bias field, and MICO, RCLFCM and MPCFCM can achieve good segmentation results under uneven intensity. Among them, MPCFCM retains the original image information to a large extent in the segmentation process. FIGURE 5, FIGURE 6 and FIGURE 7 add different bias field and noise respectively. Visually, it can be seen that with the increase of noise level, LINC and MICO are sensitive to noise, NLFCM, FRFCM and DSFCM_N are greatly affected by bias field, RCLFCM is not accurate in image details processing, and the results are not ideal, while MPCFCM can effectively retain image details, compared with the real results, the tissue segmentation is more accurate.

B. QUANTITATIVE EVALUATION

In order to evaluate the experimental results of our algorithm quantitatively, we use Jaccard similarity (*JS*) [37] as a measure and compare our experimental results with other ten algorithms. The results show that MPCFCM is more accurate and effective in tissue segmentation of brain images. The metric of *JS* is defined as follows:

$$J(S_1, S_2) = \frac{|S_1 \cap S_2|}{|S_1 \cup S_2|}. \tag{32}$$

where $|\cdot|$ represents the area of the region, S_1 is the area segmented by the algorithm, and S_2 is the corresponding area in the real image. When the value of *JS* is closer to 1, the segmentation effect is better.

We use this index as a metric to measure the segmentation accuracy of each algorithm, and compare our algorithm with the other ten algorithms. It can be found that MPCFCM can still segment the brain tissue more accurately under the influence of different noises. The quantitative results are listed in TABLE 1.

Secondly, we use Dice similarity coefficient (*DSC*) [38] to calculate the similarity of the two samples. The DSC similarity metric is defined as follows:

$$DSC(S_1, S_2) = \frac{2|S_1 \cap S_2|}{|S_1| + |S_2|} \tag{33}$$

where S_1 and S_2 correspond to the result of the algorithm and ground truth, respectively. $|S_1 \cap S_2|$ represents the number of common pixels contained in the two sets, and $|S_1| + |S_2|$ represents the total number of pixels in the two sets. A larger Dice value corresponds to a better segmentation result.

We use this index as a set of similarity metrics and compare our algorithm with ten other algorithms. Similarly, MPCFCM algorithm still has a high DSC value under the influence of different noises, indicating that MPCFCM algorithm is closer to Ground truth. The quantitative results are listed in TABLE 2.

For brain images, this paper uses two cluster validity function evaluation indexes V_{pc} and V_{pe} to evaluate the segmentation effects of various algorithms. Where V_{pc} presents the partition coefficient and V_{pe} represents the partition entropy. They are defined as follows [39]:

$$V_{pc} = \sum_{k=1}^{K} \sum_{i=1}^{N} \frac{u_{ki}^2}{N}, \tag{34}$$

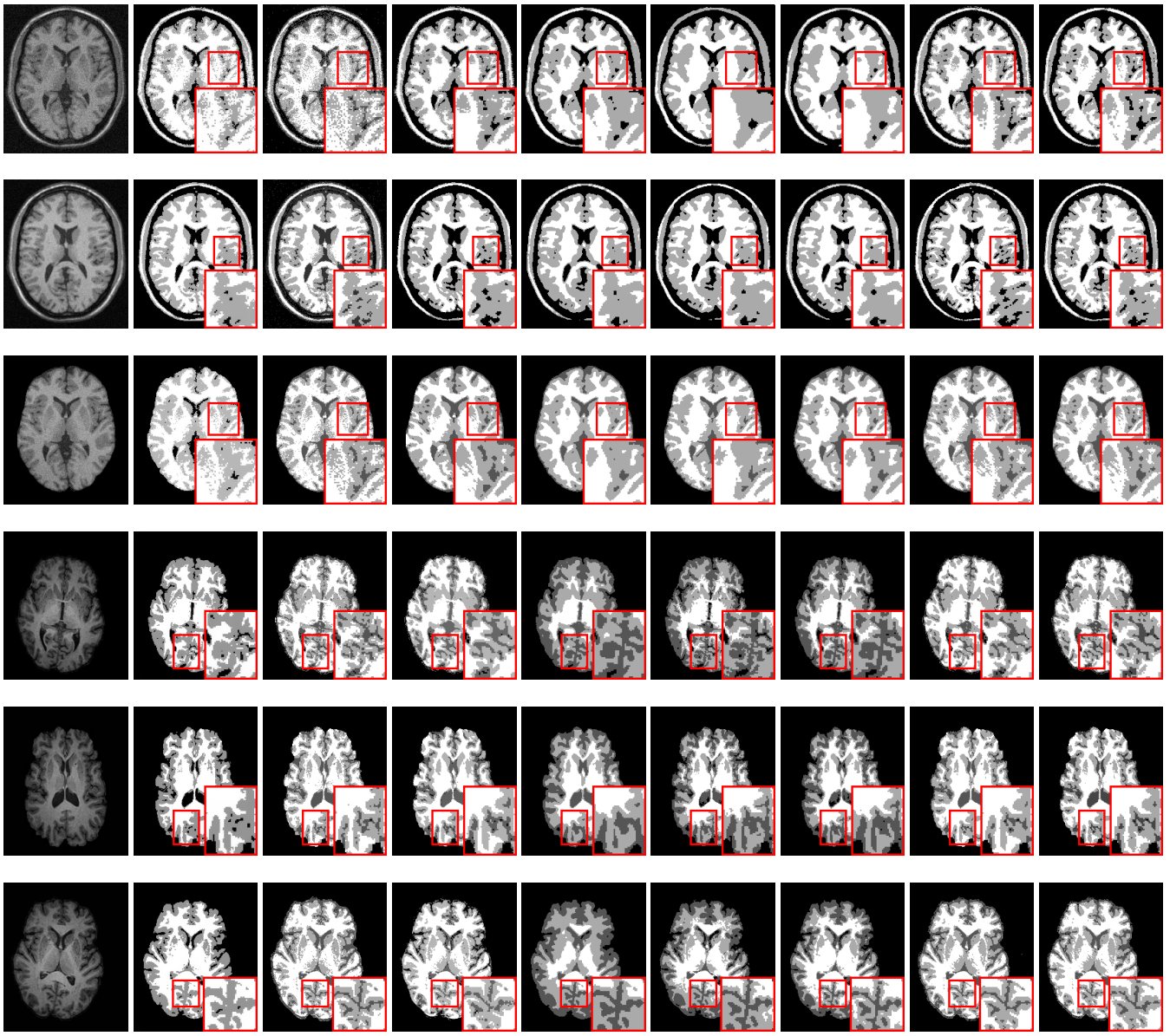

FIGURE 7. Comparison of segmentation results for different algorithms. (a) From top to bottom: brain images of T1 weighted, 1mm thick, 40% bias field and 9% Gaussian noise, 20% bias field and 7% Gaussian noise, 40% bias field and 7% Gaussian noise, 40% bias field and 5% Gaussian noise, 20% bias field and 5% Gaussian noise, 40% bias field and 3% Gaussian noise; (b) LINC; (c) MICO; (d) RCLFCM; (e) NLFCM; (f) FRFCM; (g) DSFCM_N; (h) MPCFCM; (i) Ground truth.

$$V_{pe} = -\sum_{k=1}^{K}\sum_{i=1}^{N}\frac{u_{ki}\log\left(u_{ki}\right)}{N}. \tag{35}$$

where u_{ki} represents the fuzzy membership of the pixel i belonging to the k-th fitting plane, K represents the number of clusters, and N is the total number of image pixels. In the process of algorithm segmentation, when V_{pc} obtains a high value and V_{pe} obtains a low value, it indicates that the fuzzyness of the fuzzy membership of the algorithm is smaller in the segmentation result, and the classification effect is better. This paper evaluates the effectiveness of various algorithms by comparing V_{pc} and V_{pe} of different algorithms. By comparing the data, it can be seen that MPCFCM algorithm has higher V_{pc} value and lower V_{pe} value than the other nine algorithms. Therefore, the algorithm of this paper is more accurate and effective for the organization of brain images. The quantitative results are listed in TABLE 3 and TABLE 4.

By calculating the evaluation algorithm index, we can see that our algorithm has higher V_{pc} value and lower V_{pe} value. However, when both V_{pc} and V_{pe} values are high or low, the above table is difficult to give an intuitive representation of the merits of the algorithm. Therefore, in order to see the

TABLE 1. Comparison of segmentation accuracy index (*JS*) for different algorithms.

Noise(%)	Tissum	Algorithm									
		FCM_S	EnFCM	FLICM	LIC	LINC	MICO	RCLFCM	NLFCM	FRFCM	DSFCM_N	MPCFCM
0	WM	0.9711	0.9589	0.9685	0.7835	0.7954	0.9703	**0.9869**	0.9597	0.9759	0.9721	0.9706
	GM	0.9544	0.9439	0.9598	0.7751	0.7759	0.9755	0.9757	0.9511	0.9659	0.9582	**0.9872**
	CSF	0.9803	0.9815	0.9807	0.9159	0.9258	0.9963	0.9783	0.9478	0.9887	0.9831	**0.9966**
3	WM	0.9707	0.9445	0.9678	0.7817	0.7878	0.9702	0.9737	0.9461	0.9740	0.9683	**0.9774**
	GM	0.9439	0.9442	0.9509	0.7752	0.7754	0.9669	0.9671	0.9478	0.9632	0.9508	**0.9693**
	CSF	0.9841	0.9786	0.9855	0.9134	0.9233	0.9807	0.9859	0.9375	**0.9879**	0.9788	0.9822
5	WM	0.9601	0.9363	0.9611	0.7739	0.7861	0.9537	0.9594	0.9413	0.9608	0.9611	**0.9634**
	GM	0.9412	0.9431	0.9499	0.7746	0.7749	0.9656	0.9633	0.9452	0.9593	0.9466	**0.9669**
	CSF	0.9602	0.9681	0.9714	0.9127	0.9165	0.9706	0.9719	0.9417	0.9665	**0.9727**	0.9721

TABLE 2. Comparison of similarity metrics (*DSC*) of different algorithms.

IMAGE	Noise(%)	Algorithm										
		FCM_S	EnFCM	FLICM	LIC	LINC	MICO	RCLFCM	NLFCM	FRFCM	DSFCM_N	MPCFCM
FIGURE 4	0	0.9335	0.9115	0.9271	0.8854	0.8941	0.9464	0.9502	0.9196	0.9432	0.9291	**0.9778**
		0.9474	0.9546	0.9398	0.9025	0.9240	**0.9653**	0.9593	0.9329	0.9529	0.9443	0.9645
		0.9302	0.9285	0.9222	0.8936	0.9211	0.9502	**0.9505**	0.9160	0.9378	0.9270	0.9503
FIGURE 5	3	0.9315	0.8953	0.9252	0.8813	0.8839	0.9307	0.9358	0.9179	0.9347	0.9276	**0.9596**
		0.9455	0.9369	0.9380	0.8974	0.9115	0.9500	0.9524	0.9304	0.9501	0.9437	**0.9603**
		0.9283	0.9235	0.9209	0.8833	0.9057	0.9403	**0.9465**	0.9161	0.9343	0.9263	0.9463
FIGURE 6	5	0.9274	0.8741	0.9229	0.8794	0.8753	0.9154	0.9252	0.9063	0.9278	0.9233	**0.9388**
		0.9428	0.9113	0.9372	0.8696	0.8898	0.9387	0.9457	0.9287	0.9439	0.9421	**0.9587**
		0.9263	0.9132	0.9199	0.8666	0.8906	0.9198	0.9390	0.9087	0.9283	0.9257	**0.9459**

TABLE 3. Comparison of medical image partition coefficients V_{pc}.

IMAGE	Noise(%)	Algorithm										
		FCM_S	EnFCM	FLICM	LIC	LINC	MICO	RCLFCM	NLFCM	FRFCM	DSFCM_N	MPCFCM
FIGURE 4	0	0.8622	0.7362	0.9084	0.8513	0.8737	0.8817	0.9557	0.9186	0.7808	0.8731	**0.9568**
		0.8844	0.7283	0.9201	0.8762	0.8789	0.8901	**0.9591**	0.9256	0.8107	0.8888	0.9583
		0.8902	0.7792	0.9270	0.8653	0.8705	0.8925	0.9551	0.9279	0.8211	0.8924	**0.9647**
FIGURE 5	3	0.8521	0.7312	0.9049	0.8421	0.8577	0.8653	0.9555	0.9113	0.7746	0.8673	**0.9562**
		0.8771	0.7139	0.9178	0.8642	0.8698	0.8901	0.9575	0.9214	0.8041	0.8856	**0.9577**
		0.8823	0.7753	0.9247	0.8544	0.8501	0.8704	0.9433	0.9272	0.8142	0.8874	**0.9556**
FIGURE 6	5	0.8347	0.7311	0.8989	0.8359	0.8517	0.8401	0.9532	0.9088	0.7669	0.8619	**0.9544**
		0.8637	0.7118	0.9135	0.8401	0.8505	0.8583	0.9562	0.9183	0.7959	0.8816	**0.9567**
		0.8698	0.7645	0.9206	0.8298	0.8341	0.8429	0.9401	0.9198	0.8079	0.8833	**0.9548**

superiority of the algorithm more intuitively. We combine the two indicators to redefine a new indicator to show the performance of each algorithm more intuitively. The new indicator V_{ps} is defined as follows:

$$V_{ps} = \frac{V_{pc}}{V_{pe}} = \frac{\sum_{k=1}^{K}\sum_{i=1}^{N} u_{ki}^2/N}{-\sum_{k=1}^{K}\sum_{i=1}^{N} u_{ki}\log\left(u_{ki}\right)/N} \tag{36}$$

The index is determined by the ratio of V_{pc} and V_{pe}. When V_{pc} is higher and V_{pe} is lower, the performance of the algorithm is better. When the performance metrics of the two algorithms are close, we can further judge the performance of the algorithm by comparing the values of V_{ps}. FIGURE 8 visually shows the V_{ps} values of segmentation results of different algorithms with the increase of noise. It can be seen from the figure that our algorithm still has a high V_{ps} value and the segmentation results are more accurate.

Finally, we calculate the time complexity of each algorithm. As shown in FIGURE 9, the calculation time increases with the size of the image. Among them, the quickest algorithm is EnFCM, while the slowest algorithm is FLICM. In contrast, The proposed method MPCFCM is

TABLE 4. Comparison of medical image partition entropy V_{pe}.

IMAGE	Noise(%)	Algorithm										
		FCM_S	EnFCM	FLICM	LIC	LINC	MICO	RCLFCM	NLFCM	FRFCM	DSFCM_N	MPCFCM
		0.3805	0.5796	0.2523	0.2431	0.2389	0.2243	0.0726	0.2257	0.4241	0.2445	**0.0711**
FIGURE 4	0	0.3221	0.5852	0.2199	0.2267	0.2181	0.2076	**0.0676**	0.2161	0.3713	0.2152	0.0689
		0.3048	0.4882	0.2017	0.2218	0.2165	0.2071	0.0741	0.2070	0.3499	0.2076	**0.0582**
		0.4088	0.5763	0.2624	0.2563	0.2595	0.2547	0.0734	0.2471	0.4345	0.2560	**0.0724**
FIGURE 5	3	0.3441	0.6074	0.2273	0.2302	0.2223	0.2114	**0.0699**	0.2480	0.3831	0.2226	**0.0699**
		0.3282	0.4969	0.2091	0.2593	0.2527	0.2464	0.0948	0.2390	0.3628	0.2183	**0.0733**
		0.4531	0.5748	0.2796	0.3218	0.2893	0.2973	0.0773	0.2674	0.4474	0.2665	**0.0757**
FIGURE 6	5	0.3803	0.6098	0.2406	0.2764	0.2671	0.2668	0.0723	0.2571	0.3972	0.2313	**0.0719**
		0.3621	0.5167	0.2214	0.3159	0.3119	0.2939	0.1007	0.2497	0.3742	0.2269	**0.0744**

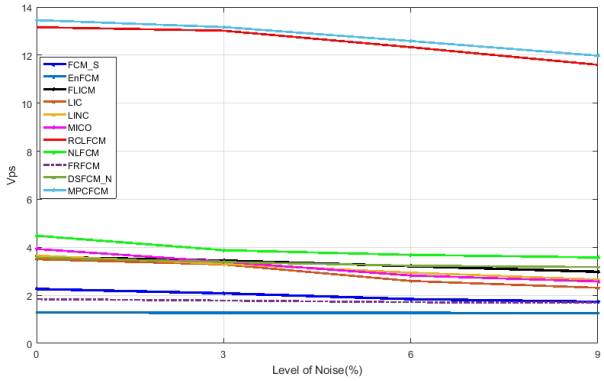

FIGURE 8. The V_{ps} values for different segmentation algorithm results as noise.

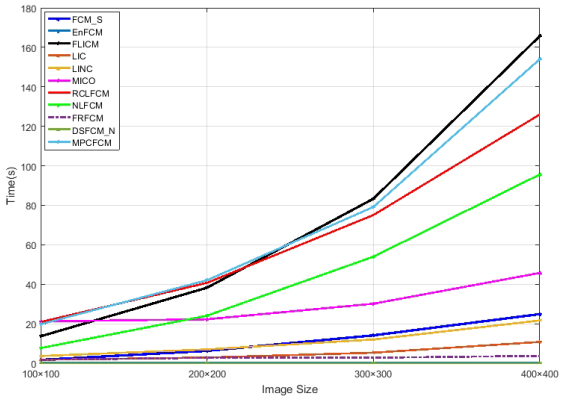

FIGURE 9. Computational cost (in second) of the eleven algorithms.

time-consuming to calculate, but it can well suppress noise and process bias field images, and MPCFCM is relatively easy to implement.

V. CONCLUSION

In this paper, we propose a new medical image segmentation method (MPCFCM) with anti-noise and bias field correction. In order to reduce the effect of intensity unevenness, a new objective function based on FCM algorithm is proposed. The new objective function takes the plane as hyper-center of clustering and completes the data point clustering by optimizing different plane coefficients iteratively. Since bias field model is included in the objective function, bias field can be corrected while the image segmentation is completed. In addition, this paper gives full consideration to the influence of neighborhood pixel information on the segmentation of pixels, and constructs a new anti-noise smoothing factor to suppress noise effectively and retain image details. Finally, we have further detailed processing on the segmented image so that the segmented image can retain more image detail information. The proposed algorithm is compared with the other ten algorithms. Experimental results show that MPCFCM can estimate the bias field and suppress noise effectively, and can get more accurate segmentation results.

However, MPCFCM algorithm still has some shortcomings: (1) The algorithm has higher time complexity; (2) The algorithm does not achieve the desired results in processing natural images. Next, we will further improve the algorithm, improve the segmentation accuracy of the algorithm, use quadratic polynomial surface fitting, and improve the universality of the algorithm while reducing the time complexity.

REFERENCES

[1] J. C. Bezdek, *Pattern Recognition With Fuzzy Objective Function Algorithms*. New York, NY, USA: Springer, 2013.

[2] M. N. Ahmed, S. M. Yamany, N. Mohamed, A. A. Farag, and T. Moriarty, "A modified fuzzy C-means algorithm for bias field estimation and segmentation of MRI data," *IEEE Trans. Med. Imag.*, vol. 21, no. 3, pp. 193–199, Mar. 2002.

[3] M. A. Balafar, A. R. Ramli, S. Mashohor, and A. Farzan, "Compare different spatial based fuzzy-C_mean (FCM) extensions for MRI image segmentation," in *Proc. 2nd Int. Conf. Comput. Autom. Eng. (ICCAE)*, vol. 5, Feb. 2010, pp. 609–611.

[4] S. Chen and D. Zhang, "Robust image segmentation using FCM with spatial constraints based on new kernel-induced distance measure," *IEEE Trans. Syst., Man, Cybern. B. Cybern.*, vol. 34, no. 4, pp. 1907–1916, Aug. 2004.

[5] L. Szilagyi, Z. Benyo, S. M. Szilagyi, and H. S. Adam, "MR brain image segmentation using an enhanced fuzzy C-means algorithm," in *Proc. 25th Annu. Int. Conf. IEEE Eng. Med. Biol. Soc.*, vol. 1, Sep. 2003, pp. 724–726.

[6] S. Krinidis and V. Chatzis, "A robust fuzzy local information C-means clustering algorithm," *IEEE Trans. Image Process.*, vol. 19, no. 5, pp. 1328–1337, May 2010.

[7] C. L. Chowdhary and D. P. Acharjya, "Breast cancer detection using intuitionistic fuzzy histogram hyperbolization and possibilitic fuzzy C-mean clustering algorithms with texture feature based classification on mammography images," in *Proc. Int. Conf. Adv. Inf. Commun. Technol. Comput. (AICTC)*, 2016, pp. 1–6.
[8] C. L. Chowdhary, G. V. K. Sai, and D. P. Acharjya, "Decreasing false assumption for improved breast cancer detection," *J. Sci. Arts*, vol. 35, no. 2, pp. 157–176, 2016.
[9] C. L. Chowdhary and D. P. Acharjya, "A hybrid scheme for breast cancer detection using intuitionistic fuzzy rough set technique," *Int. J. Healthcare Inf. Syst. Informat.*, vol. 11, no. 2, pp. 38–61, Apr. 2016.
[10] C. L. Chowdhary, G. V. K. Sai, and D. Acharjya, "Decrease in false assumption for detection using digital mammography," in *Computational Intelligence in Data Mining*, vol. 411. New Delhi, India: Springer, 2016, pp. 325–333.
[11] D. P. Acharjya and C. L. Chowdhary, "Breast cancer detection using hybrid computational intelligence techniques," in *Handbook of Research on Emerging Perspectives on Healthcare Information Systems and Informatics*. Hershey, PA, USA: IGI Global, 2018, pp. 251–280.
[12] C. L. Chowdhary and D. P. Acharjya, "Segmentation of mammograms using a novel intuitionistic possibilistic fuzzy C-mean clustering algorithm," in *Nature Inspired Computing*. New York, NY, USA: Springer, 2018, pp. 75–82.
[13] S. Roy and P. Maji, "Medical image segmentation by partitioning spatially constrained fuzzy approximation spaces," *IEEE Trans. Fuzzy Syst.*, vol. 28, no. 5, pp. 965–977, May 2020.
[14] C. Li, R. Huang, Z. Ding, J. C. Gatenby, D. N. Metaxas, and J. C. Gore, "A level set method for image segmentation in the presence of intensity inhomogeneities with application to MRI," *IEEE Trans. Image Process.*, vol. 20, no. 7, pp. 2007–2016, Jul. 2011.
[15] C. Feng, D. Zhao, and M. Huang, "Image segmentation and bias correction using local inhomogeneous iNtensity clustering (LINC): A region-based level set method," *Neurocomputing*, vol. 219, pp. 107–129, Jan. 2017.
[16] X. Lu, X. Zhang, M. Li, Z. Zhang, and H. Xu, "A level set method combined with Gaussian mixture model for image segmentation," in *Proc. Chin. Conf. Pattern Recognit. Comput. Vis. (PRCV)*. Cham, Switzerland: Springer, 2019, pp. 185–196.
[17] C. L. Chowdhary and D. P. Acharjya, "Clustering algorithm in possibilistic exponential fuzzy C-mean segmenting medical images," *J. Biomimetics, Biomater. Biomed. Eng.*, vol. 30, pp. 12–23, Jan. 2017.
[18] C. Feng, D. Zhao, and M. Huang, "Image segmentation using CUDA accelerated non-local means denoising and bias correction embedded fuzzy c-means (BCEFCM)," *Signal Process.*, vol. 122, pp. 164–189, May 2016.
[19] C. Feng, D. Zhao, and M. Huang, "Segmentation of longitudinal brain MR images using bias correction embedded fuzzy C-means with non-locally spatio-temporal regularization," *J. Vis. Commun. Image Represent.*, vol. 38, pp. 517–529, Jul. 2016.
[20] C. Feng, W. Li, J. Hu, K. Yu, and D. Zhao, "BCEFCM_S: Bias correction embedded fuzzy C-means with spatial constraint to segment multiple spectral images with intensity inhomogeneities and noises," *Signal Process.*, vol. 168, Mar. 2020, Art. no. 107347.
[21] Y. LeCun, Y. Bengio, and G. Hinton, "Deep learning," *Nature*, vol. 521, pp. 436–444, May 2015.
[22] D. Shen, G. Wu, and H. I. Suk, "Deep learning in medical image analysis," *IEEE Trans. Biomed. Eng.*, vol. 19, no. 1, pp. 221–248, Jun. 2017.
[23] J. H. Thrall, X. Li, Q. Li, C. Cruz, S. Do, K. Dreyer, and J. Brink, "Artificial intelligence and machine learning in radiology: Opportunities, challenges, pitfalls, and criteria for success," *J. Amer. College Radiol.*, vol. 15, no. 3, pp. 504–508, Mar. 2018.
[24] B. H. Menze *et al.*, "The multimodal brain tumor image segmentation benchmark (BRATS)," *IEEE Trans. Med. Imag.*, vol. 34, no. 10, pp. 1993–2024, Oct. 2015.
[25] M. Havaei, A. Davy, D. Warde-Farley, A. Biard, A. Courville, Y. Bengio, C. Pal, P.-M. Jodoin, and H. Larochelle, "Brain tumor segmentation with deep neural networks," *Med. Image Anal.*, vol. 35, pp. 18–31, Jan. 2017.
[26] S. Pereira, A. Pinto, V. Alves, and C. A. Silva, "Brain tumor segmentation using convolutional neural networks in MRI images," *IEEE Trans. Med. Imag.*, vol. 35, no. 5, pp. 1240–1251, May 2016.
[27] S. Prima, N. Ayache, T. Barrick, and N. Roberts, "Maximum likelihood estimation of the bias field in MR brain images: Investigating different modelings of the imaging process," in *Proc. Int. Conf. Med. Image Comput. Comput.-Assist. Intervent. (MICCAI)*. Utrecht, The Netherlands: Springer, 2001, pp. 811–819.
[28] C. Li, C. Gatenby, L. Wang, and J. C. Gore, "A robust parametric method for bias field estimation and segmentation of MR images," in *Proc. IEEE Conf. Comput. Vis. Pattern Recognit.*, Jun. 2009, pp. 218–223.
[29] M. J. D. Powell, *Approximation Theory and Methods*. Cambridge, U.K.: Cambridge Univ. Press, 1981.
[30] Q. Guo, C. Zhang, Y. Zhang, and H. Liu, "An efficient SVD-based method for image denoising," *IEEE Trans. Circuits Syst. Video Technol.*, vol. 26, no. 5, pp. 868–880, May 2016.
[31] (Apr. 2016). *BrainWeb: Simulated Brain Database*. [Online]. Available: http://brainweb.bic.mni.mcgill.ca/brainweb/
[32] C. Li, J. C. Gore, and C. Davatzikos, "Multiplicative intrinsic component optimization (MICO) for MRI bias field estimation and tissue segmentation," *Magn. Reson. Imag.*, vol. 32, no. 7, pp. 913–923, Sep. 2014.
[33] W.-Q. Deng, X.-M. Li, X. Gao, and C.-M. Zhang, "A modified fuzzy C-means algorithm for brain MR image segmentation and bias field correction," *J. Comput. Sci. Technol.*, vol. 31, no. 3, pp. 501–511, May 2016.
[34] X. Zhang, Y. Sun, G. Wang, Q. Guo, C. Zhang, and B. Chen, "Improved fuzzy clustering algorithm with non-local information for image segmentation," *Multimedia Tools Appl.*, vol. 76, no. 6, pp. 7869–7895, Mar. 2017.
[35] T. Lei, X. Jia, Y. Zhang, L. He, H. Meng, and A. K. Nandi, "Significantly fast and robust fuzzy C-Means clustering algorithm based on morphological reconstruction and membership filtering," *IEEE Trans. Fuzzy Syst.*, vol. 26, no. 5, pp. 3027–3041, Oct. 2018.
[36] Y. Zhang, X. Bai, R. Fan, and Z. Wang, "Deviation-sparse fuzzy C-means with neighbor information constraint," *IEEE Trans. Fuzzy Syst.*, vol. 27, no. 1, pp. 185–199, Jan. 2019.
[37] D. W. Shattuck, S. R. Sandor-Leahy, K. A. Schaper, D. A. Rottenberg, and R. M. Leahy, "Magnetic resonance image tissue classification using a partial volume model," *NeuroImage*, vol. 13, no. 5, pp. 856–876, May 2001.
[38] A. W.-C. Liew and H. Yan, "An adaptive spatial fuzzy clustering algorithm for 3-D MR image segmentation," *IEEE Trans. Med. Imag.*, vol. 22, no. 9, pp. 1063–1075, Sep. 2003.
[39] J. C. Bezdek, "Cluster validity with fuzzy sets," *J. Cybern.*, vol. 3, no. 3, pp. 58–73, Jan. 1973.

HONG XU received the B.S. degree in computer application technology from the Zhejiang University of Science and Technology, in 1990, and the M.S. degree in computer application technology from Shandong University, in 2002. She was a Visiting Scholar with The City University of New York, in 2010. She is currently a Professor and the Vice President of the Shandong Institute of Commerce and Technology. Her research interests include information visualization, image processing, cloud computing technology applications, and education informatization.

CAIZENG YE received the B.S. degree in computer science and technology from the University of Jinan, Jinan, China, in 2014. He is currently pursuing the M.S. degree with the School of Computer Science and Technology, Shandong University, Jinan. His research interests include medical image processing and computer vision.

FAN ZHANG received the B.S. and Ph.D. degrees in computer science from Shandong University, in 2009 and 2015, respectively. From 2012 to 2014, he was invited to visit the Department of Computer Science, University of Kentucky, USA, as a joint training Ph.D. Student. He is currently an Associate Professor with the School of Computer Science and Technology, Shandong Technology and Business University. His research interests include image processing, computer vision, computer graphics, and CAGD.

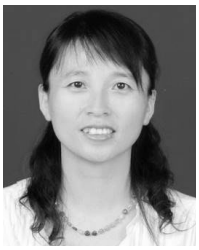

XUEMEI LI received the master's and Ph.D. degrees from Shandong University, Jinan, China, in 2004 and 2010, respectively. From 2013 to 2014, she was a Visiting Scholar with the University of Houston, USA. She is currently an Associate Professor with the School of Software, Shandong University, and a member of the GD&IV Laboratory. She is engaged in research on geometric modeling, CAGD, medical image processing, and information visualization.

CAIMING ZHANG received the B.S. and M.S. degrees in computer science from Shandong University, Jinan, China, in 1982 and 1984, respectively, and the Ph.D. degree in computer science from the Tokyo Institute of Technology, Tokyo, Japan, in 1994. From 1998 to 1999, he was a Postdoctoral Fellow of the University of Kentucky, Lexington, USA. He is currently a Professor with the School of Software, Shandong University, and a Distinguished Professor with the School of Computer Science and Technology, Shandong University of Finance and Economics. His research interests include CAGD, information visualization, and medical image processing.